Eur. Phys. J. Plus (2017) **132**: 520
DOI 10.1140/epjp/i2017-11801-5

THE EUROPEAN PHYSICAL JOURNAL PLUS

Regular Article

Studies of the micromorphology of sputtered TiN thin films by autocorrelation techniques

Kamil Smagoń[1], Sebastian Stach[1], Ştefan Ţălu[2,a], Ali Arman[3], Amine Achour[4], Carlos Luna[5], Nader Ghobadi[6], Mohsen Mardani[3], Fatemeh Hafezi[3], Azin Ahmadpourian[7,b], Mohsen Ganji[5], and Alireza Grayeli Korpi[8]

[1] University of Silesia, Faculty of Computer Science and Materials Science, Institute of Informatics, Department of Biomedical Computer Systems, Będzińska 39, 41-205 Sosnowiec, Poland
[2] Technical University of Cluj-Napoca, The Directorate of Research, Development and Innovation Management (DMCDI), Constantin Daicoviciu Street, no. 15, Cluj-Napoca, 400020, Cluj county, Romania
[3] Vacuum Technology Group, ACECR - Sharif Branch, Tehran, Iran
[4] Institut National de la Recherche Scientifique (INRS) 1650 Boulevard Lionel - Boulet, Varennes, Canada
[5] Universidad Autónoma de Nuevo León (UANL), Facultad de Ciencias Físico Matemáticas (FCFM), Av. Universidad s/n, San Nicolás de los Garza Nuevo León, Mexico
[6] Physics Department, Faculty of Science, Malayer University, Malayer, Iran
[7] Young Researchers and Elite Club, Arak Branch, Islamic Azad University, Arak, Iran
[8] Physics and Accelerators Research School, Nuclear Sciences and Technology Research Institute, Tehran, Iran

Received: 14 April 2017 / Revised: 18 July 2017
Published online: 14 December 2017 – © Società Italiana di Fisica / Springer-Verlag 2017

Abstract. Autocorrelation techniques are crucial tools for the study of the micromorphology of surfaces: They provide the description of anisotropic properties and the identification of repeated patterns on the surface, facilitating the comparison of samples. In the present investigation, some fundamental concepts of these techniques including the autocorrelation function and autocorrelation length have been reviewed and applied in the study of titanium nitride thin films by atomic force microscopy (AFM). The studied samples were grown on glass substrates by reactive magnetron sputtering at different substrate temperatures (from 25 °C to 400 °C), and their micromorphology was studied by AFM. The obtained AFM data were analyzed using MountainsMap Premium software obtaining the correlation function, the structure of isotropy and the spatial parameters according to ISO 25178 and EUR 15178N. These studies indicated that the substrate temperature during the deposition process is an important parameter to modify the micromorphology of sputtered TiN thin films and to find optimized surface properties. For instance, the autocorrelation length exhibited a maximum value for the sample prepared at a substrate temperature of 300 °C, and the sample obtained at 400 °C presented a maximum angle of the direction of the surface structure.

1 Introduction

Physics of thin films is an important branch of solid state physics that has been prominently developed in recent years. It deals with systems that, although they can exhibit a large variety of physical properties, they have a feature in common: one of their three dimensions is on the nanoscale.

Due to their mechanical properties, high hardness and high thermal and chemical stability, titanium nitride thin films are used in the industry as wear-resistant protective coating in car parts, cutting tools and decorative layers [1–8]. Moreover, TiN coatings improve the functionality of materials by hardening them, prevent surface slip and shear, and make the coated material non-toxic; thus, it is widely used in medical devices inside body (artificial organs) and implants [9, 10].

[a] e-mail: stefan_ta@yahoo.com
[b] e-mail: azinahmadpurian@gmail.com

Several studies have shown that factors such as preferred orientation, residual stresses, grain accumulation and grain size affect significantly to the structural, semiconductor, optical and mechanical properties of TiN thin films [11–15]; therefore, engineered TiN thin films can be grown on surfaces of semiconductors with applications in catalysis, electronics, sensors like dye-sensitized solar cells and storage of electrochemical energy or hydrogen [16–22].

Titanium nitride films are chemically stable when deposited by sputtering in a wide range of nitrogen gas feed rates, resulting in stable stoichiometric ratios. However, nitrogen deficiency causes vacancies in the crystal lattice, and the formation of non-stoichiometrc layers can occur. Among the most common methods for fabricating thin films, which include the physical vapor deposition (PVD) and chemical vapor deposition (CVD) [22,23], the magnetic sputtering method stands out for its versatility that allows the production of a wide range of thin film systems with different characteristics, including metals, alloys, oxides, nitrides and carbides [24–30].

Owing to the diversity that exists in manufacturing of thin films, the determination of the surface morphology and its dependences on the preparation parameters is crucial to explain their physical properties and exploit them to improve technological applications. Hence, different methods and techniques have been performed for the study of morphological properties using microscopic analysis like atomic force microscopy (AFM) that provides key information about the surface when is combined with various analytical methods such as fractal analysis, autocorrelation and intercorrelation techniques, etc. [31–35].

In the present investigation six thin layers of titanium nitride (TiN) were prepared by reactive magnetron sputtering at substrate temperatures of 25, 100, 200, 250, 300 and 400 °C [36,37]. These samples display excellent properties for tribological applications and wear resistance that increases the service life and usefulness of the coated surface. Consequently, titanium nitride coatings are widely used in medicine for the production of tools and machine parts. Thus, morphological properties of these films are studied using autocorrelation techniques that enable the identification of similarities between samples.

1.1 Autocorrelation function

Autocorrelation function (ACF) assess the correlation of a part of an image in relation to the entire image. Autocorrelation function is defined as [31]

$$\mathrm{ACF}\,(\tau_x,\tau_y)=\frac{\iint z(x,y)z(x-\tau_x,y-\tau_y)\mathrm{d}x\,\mathrm{d}y}{\iint z(x,y)^2\mathrm{d}x\,\mathrm{d}y}\,. \tag{1}$$

The ACF is found by taking a duplicate surface $(Z(x-D_x,y-D_y))$ of the measured surface $(Z(x,y))$ and mathematically multiplying the two surfaces together, with a relative lateral displacement (Dx,Dy) between the two surfaces. As a result, the autocorrelation function corresponds to the autocovariance of surface integrated and standardized by the parameter Sq [31]. The autocorrelation function provides values from -1 to $+1$ for each point on the surface.

Thus the ACF is a measure of how similar the surface texture is at a given distance from the original location. If the ACF stays near $+1$ for a given amount of shift, then the surface texture is similar along that direction. If the ACF falls rapidly to zero along a given direction, then the surface is different and thus uncorrelated with the original measurement location [30].

ACF is used to study the periodicity on the surface, that is, when the motif of a structure is repeatedly recreated at the surface to determine the surface isotropy [31].

1.2 The autocorrelation length, Sal

The auto-correlation length is defined as the horizontal distance ACF (tx,ty), which quickly breaks down to a specific value s with $0\le s<1$ [31].

The Sal value is calculated from

$$Sal=\min\sqrt{tx^2+ty^2}. \tag{2}$$

For all practical applications regarding relatively smooth surfaces, the value of the coefficient s is taken equal to 0.2 according to ISO 25178. For anisotropic surfaces, the Sal direction is perpendicular to the surface contour. High value of Sal means that the surface structure is dominated by components with low spatial frequency, while a low value of Sal implies a high spatial frequency. Therefore, Sal is a quantitative measure of the distance along the surface by which one would find a surface texture that is statistically different from the original location [31].

Table 1. Deposition parameters of samples.

Sample	Substrate temperature	Sputtring parameters			Rate	Thickness
		Basic pressure	Work pressure	Power		
	[°C]	[mbar]	[mbar]	[W]	[nm/min]	[nm]
S1	Room	4.5×10^{-5}	2×10^{-3}	350	4.7	565
S2	100	4.5×10^{-5}	2×10^{-3}	350	3.4	405
S3	200	4.5×10^{-5}	2×10^{-3}	350	5.4	650
S4	250	4.5×10^{-5}	2×10^{-3}	350	5.4	650
S5	300	4.5×10^{-5}	2×10^{-3}	350	5.4	650
S6	400	4.5×10^{-5}	2×10^{-3}	350	4	485

2 Materials and methods

2.1 Research material

TiN thin films were grown on glass substrates by standard reactive magnetron spattering techniques varying the temperature of the substrate (room temperature, 100, 200, 250, 300 and 400 °C) obtaining six samples named S1, S2, S3, S4, S5 and S6, respectively. More details of the preparation of these samples can be found elsewhere [36,37]. Experimental parameters were fixed as shown in table 1.

2.2 Research method

2.2.1 Atomic force microscope (AFM)

The surface properties of samples were investigated by atomic force microscope that belongs to a group of scanning probe microscopies (scanning probe microscope —SPM) [31].

2.2.2 Analysis of the AFM data

In order to analyze the obtained AFM images of the samples surface, we used specialized software MountainsMap® Premium 6.2, created by Digital Surf. This program is designed to analyze images of surfaces and it includes the necessary functions to analyze the structure of surfaces and the geometry in accordance with standarized norms (specifically, ISO 25178 and EUR 15178N) [38]. Initially, each test sample was subjected to leveling operations using Least Squares method by subtraction in order to get rid of a possible gradient of the surface image (fig. 1).

The next step involved the generation of an identification card. The generated identification card shows characteristic parameters of the sample, such as length, size, spacing and offset in relation to the each of the three dimensions. Tables 2–7 shows the stereometric parameters of the three-dimensional surface that were generated by the ID card for the six samples.

Then, for better illustration of the structure of the sample surfaces, three-dimensional views of the AFM were performed, including the calibration scale in micrometers (μm), the system of XYZ axes, the ratio of the image layout, block of dimensions and color palette (fig. 2). The differences in height of the surface structure are represented by a variable false color sequence.

In the next step an operation of shape removal was conducted in order to extract analyzed area and to obtain a surface image without altered characteristics (fig. 3).

Afterwards, new identification cards were performed to analyze the six surfaces after shapes removal. The results are shown in the following tables 8–13.

Moreover, the stereometric parameters of a three-dimensional surface of the six samples were generated in agreement with ISO 25178 and EUR 15178N, respectively. As an illustrative example, we present these data for the sample S1 in tables 14 and 15.

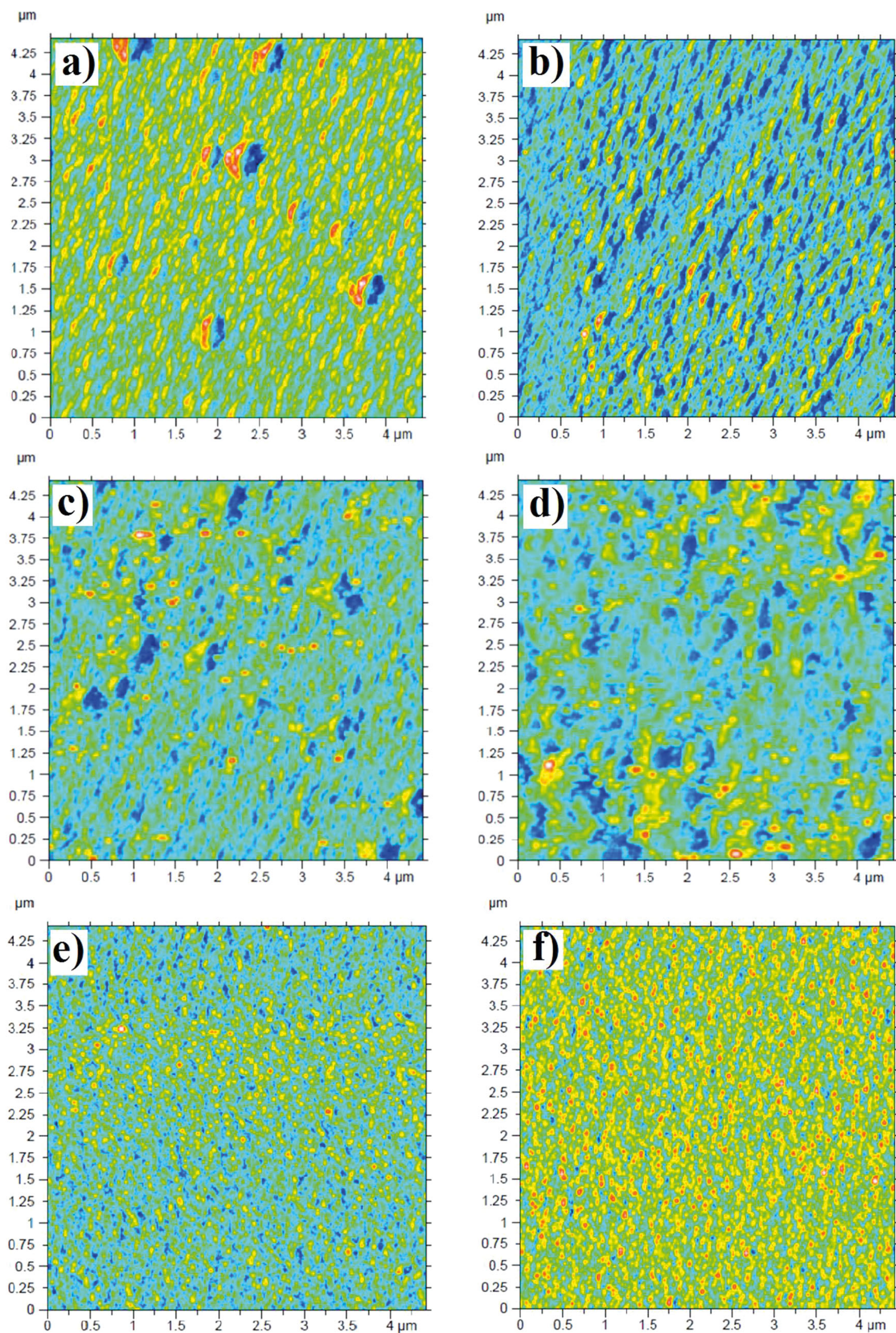

Fig. 1. Leveled AFM images of the six samples: (a) S-1; (b) S2; (c) S3; (d) S4; (e) S5; (f) S6.

Table 2. Parameters of the first sample generated from the ID card.

Parameter	Axis		
	X	Y	Z
Length [μm]	4.42	4.42	0.029
Spacing [nm]	17.3	17.3	0.0000409
Offset [μm]	0.00	−4.42	–
Min [nm]	–	–	−10.7
Max [nm]	–	–	18.3
Size	256 Points	256 Lines	708963 Decimals

Table 3. Parameters of the second sample generated from the ID card.

Parameter	Axis		
	X	Y	Z
Length [μm]	4.42	4.42	0.025
Spacing [nm]	17.3	17.3	0.0000416
Offset [μm]	0.00	−4.42	–
Min [nm]	–	–	−6.51
Max [nm]	–	–	18.5
Size	256 Points	256 Lines	601250 Decimals

Table 4. Parameters of the third sample generated from the ID card.

Parameter	Axis		
	X	Y	Z
Length [μm]	4.42	4.42	0.038
Spacing [nm]	17.3	17.3	0.000135
Offset [μm]	0.00	−4.42	–
Min [nm]	–	–	−10.8
Max [nm]	–	–	27.2
Size	256 Points	256 Lines	282560 Decimals

Table 5. Parameters of the fourth sample generated from the ID card.

Parameter	Axis		
	X	Y	Z
Length [μm]	4.42	4.42	0.0576
Spacing [nm]	17.3	17.3	0.000234
Offset [μm]	0.00	−4.42	–
Min [nm]	–	–	−15.8
Max [nm]	–	–	41.7
Size	256 Points	256 Lines	245847 Decimals

Table 6. Parameters of the fifth sample generated from the ID card.

Parameter	Axis		
	X	Y	Z
Length [μm]	4.42	4.42	0.0277
Spacing [nm]	17.3	17.3	0.0000358
Offset [μm]	0.00	-4.42	–
Min [nm]	–	–	-6.83
Max [nm]	–	–	20.9
Size	256 Points	256 Lines	774315 Decimals

Table 7. Parameters of the sixth sample generated from the ID card.

Parameter	Axis		
	X	Y	Z
Length [μm]	4.42	4.42	0.0239
Spacing [nm]	17.3	17.3	0.000127
Offset [μm]	0.00	-4.42	–
Min [nm]	–	–	-7.89
Max [nm]	–	–	16.0
Size	256 Points	256 Lines	188285 Decimals

Table 16 depicts a comparison between the spatial parameters for the first sample surface from the two standard norms (ISO 25178 and EUR 15178N). The following parameters were compared:

– Elongation of the structure (Str) is a parameter that describes the anisotropy whose value is in the range $0 < x < 1$ [38,39].

– Direction of the surface structure (Std) defines a value of an angle with respect to the maximum angular value of frequency [39].

– Length autocorrelation surface (Sal) is defined as a horizontal distance ACF (autocorrelation function), which breaks down quickly to a specific value s with $0 \leq s \leq 1$ [38,39].

– The horizontal distance of the autocorrelation function (tx, ty) has the fastest dispersion to a defined value s being $0 < s < 1$.

Differences between the Std parameter values result from the fact that during the calculations we take into account the different angle that depends on the standard used.

Further analyses were carried out with the caclulation of the autocorrelation function (ACF) that assess the correlation of one part of the AFM image in relation to the entire image [39]. Each sample was subjected to an autocorrelation operation using a threshold of 0.2 (white part is above the threshold). Figures 4(a) and (b) shows the autocorrelation peak in 2D and 3D representations, respectively, obtained for the sample S1 as a representative example.

Test samples were also analyzed in terms of the direction of structure (figs. 5(a) and (b) show the results obtained for the first sample). This study is designed to analyze surfaces along different directions. The structure was analyzed

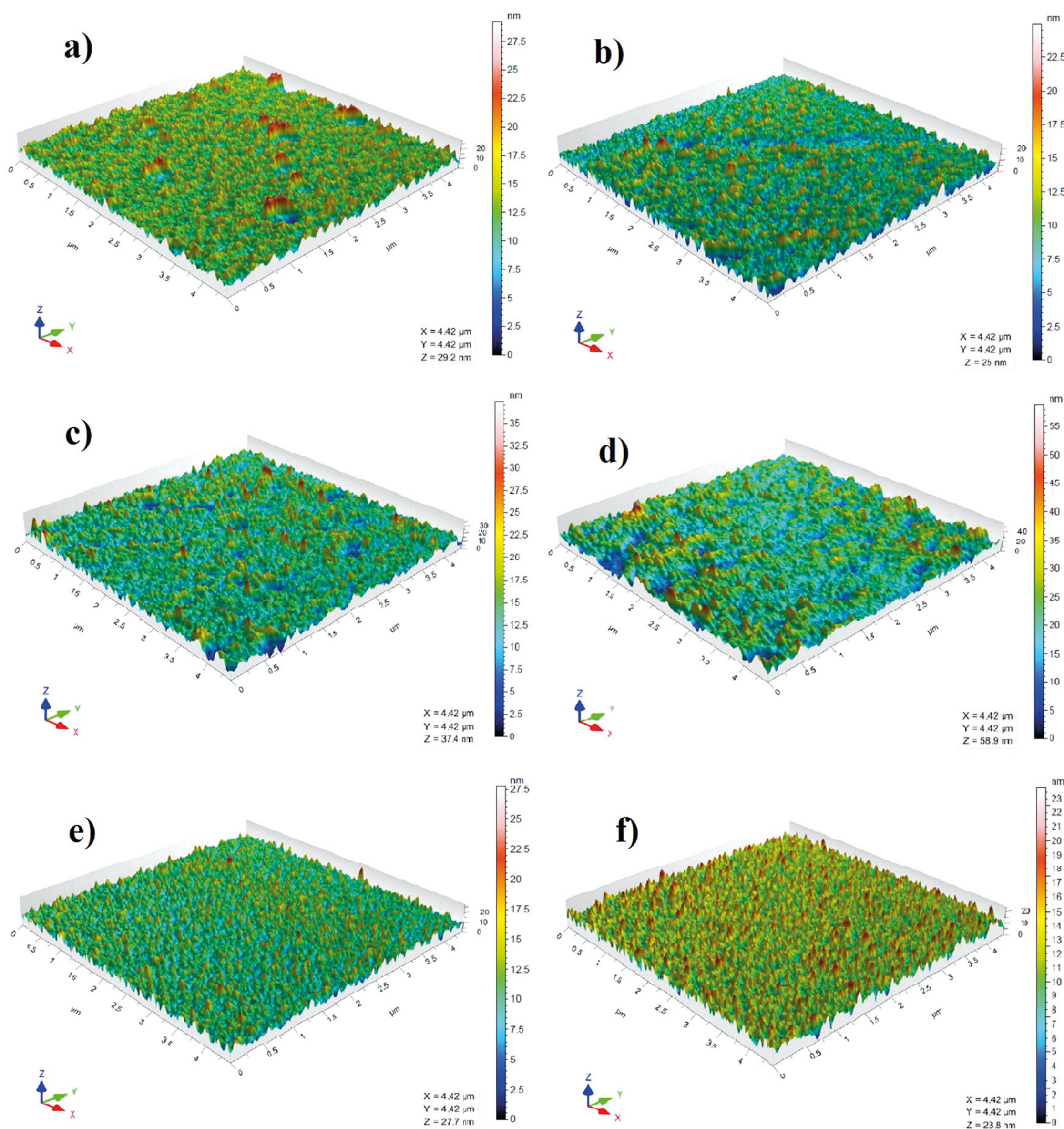

Fig. 2. Three-dimensional representations of the AFM images of the six samples: (a) S-1; (b) S2; (c) S3; (d) S4; (e) S5; (f) S6.

by Fourier transforms and angular power spectrum identifying values of the most important directions of the structure, which were located on the analyzed surface.

Directionality structure can be only examined when the value of the isotropy is below 30%, otherwise the directions may not be sufficiently important for the analysis of the surface. In the next step, the structure of the isotropy was analyzed using the autocorrelation function. The test sample was subjected to deletion of the surface shape, then calculation and optimization of surface autocorrelation was made in order to provide values in the range 0–1 (fig. 5(b)). The resulting information shows the binary autocorrelation thresholding of a surface with a default threshold of 0.2. In the case of the first sample, the isotropy is equal to 27.7%. The first direction of analyzed sample has a value of 90°, the second direction 45°, and the third direction 63.5°. The results were illustrated via the flow diagram (fig. 5(b)). The first direction has an angle with the largest power spectrum and it corresponds to the preferred direction of the surface structures. Table 17 summarizes the data obtained for the six samples.

2.3 Analysis of the results

In this research six samples were analyzed with the atomic force microscope. With the help of AFM it was possible to obtain stereometric representation of the samples and their surfaces that have been subjected to further analysis

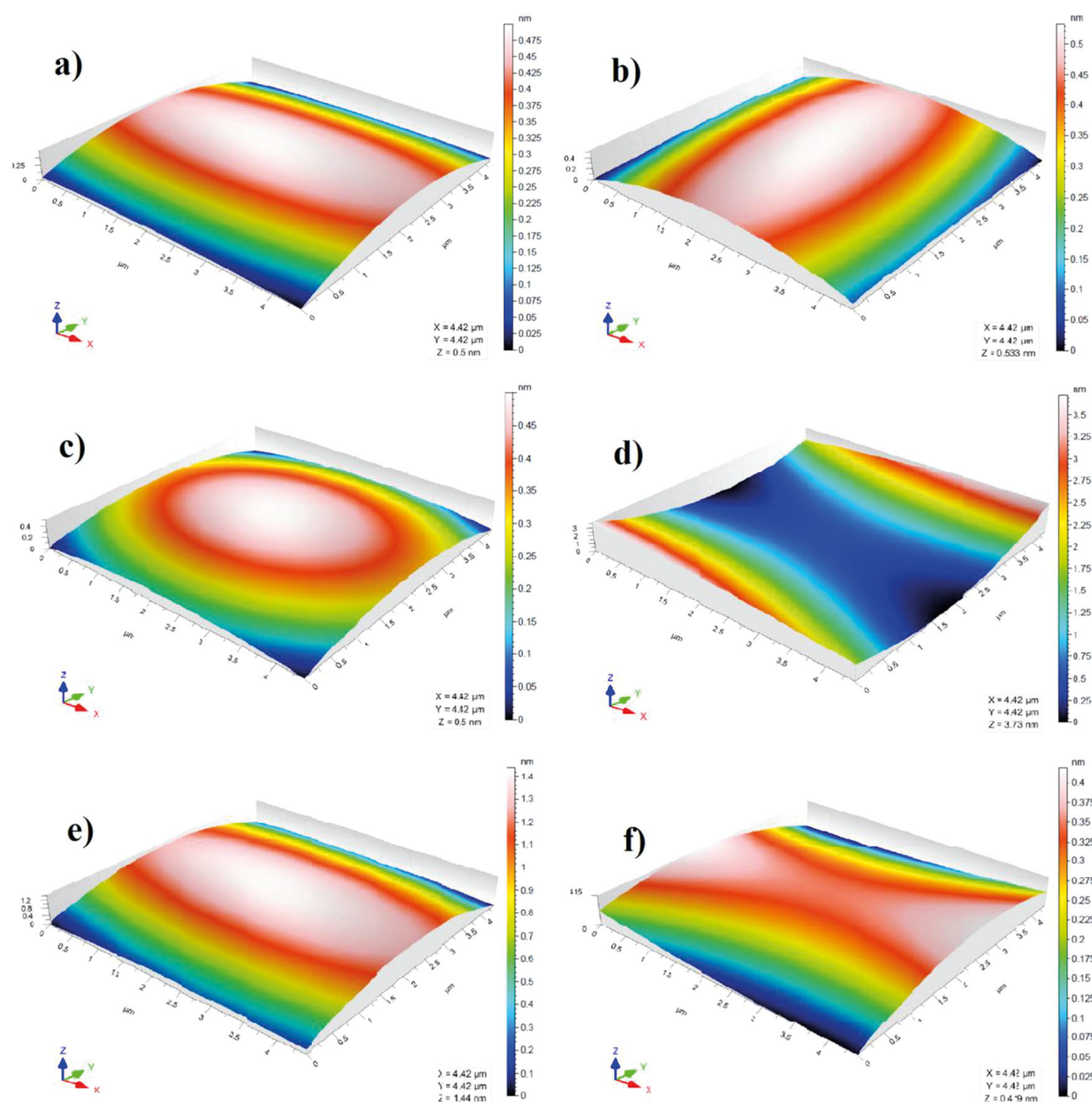

Fig. 3. 3D AFM images of the six samples after shape removal: (a) S-1; (b) S2; (c) S3; (d) S4; (e) S5; (f) S6.

in MountainsMap® Premium. Initially, each sample has been leveled with LS method by subtraction, which resulted in change of dimension of the sample relative to Z axis (fig. 1). Differences in height among samples are recorded in table 18.

After leveling, the difference in altitude increased for samples I and IV, while it decreased for the rest of samples (table 18).

Then, each of the samples received a three-dimensional visualization of surface depicting the height differences of the structure with the calibration in the scale of micrometers, stereometric tables containing the spatial parameters characterizing the topographical properties of the analyzed surfaces. Above operations were illustrated with the use of diagram (fig. 2).

Then, a table was prepared in order to record spatial parameters for the tested surfaces including two standards (tables 19 and 20).

3 Conclusions

Autocorrelation techniques have been used in the study of the surface micromorphology of TiN thin films prepared by reactive magnetron sputtering under different substrate temperatures (from 25 °C to 400 °C).

Table 8. Parameters of the first sample generated from the ID card after shapes removal.

Parameter	Axis		
	X	Y	Z
Length [μm]	4.42	4.42	0.0292
Spacing [nm]	17.3	17.3	0.0000409
Offset [μm]	0.00	−4.42	–
Min [nm]	–	–	−12.2
Max [nm]	–	–	17.0
Size	256 Points	256 Lines	713540 Decimals

Table 9. Parameters of the second sample generated from the ID card after shape removal.

Parameter	Axis		
	X	Y	Z
Length [μm]	4.42	4.42	0.025
Spacing [nm]	17.3	17.3	0.0000416
Offset [μm]	0.00	−4.42	–
Min [nm]	–	–	−7.93
Max [nm]	–	–	17.0
Size	256 Points	256 Lines	600566 Decimals

Table 10. Parameters of the third sample generated from the ID card after shape removal.

Parameter	Axis		
	X	Y	Z
Length [μm]	4.42	4.42	0.0374
Spacing [nm]	17.3	17.3	0.000135
Offset [μm]	0.00	−4.42	–
Min [nm]	–	–	−12.8
Max [nm]	–	–	24.7
Size	256 Points	256 Lines	278241 Decimals

Spatial parameter Str takes values in the range 0–1. If the value of the parameter takes values which are close to 1, then this proves the fact that the surface is isotropic, as well as, that structure is the same in all directions. If the parameter value is close to 0 —this indicates the anisotropic surface-which is periodically oriented.

Isotropic surfaces, which take values close to 100% show a more rounded flap, while the anisotropic surfaces are close to 0%. Directionality structure is examined when the value of the isotropy is below 30%, otherwise the directions may not be sufficiently important for the analysis of the surface. These research is designed to analyze the surface of the main directions, which are, inter alia, scratches —then the structure is analyzed via the Fourier transform, as well as the angular power spectrum.

Table 11. Parameters of the fourth sample generated from the ID card after shape removal.

Parameter	Axis		
	X	Y	Z
Length [μm]	4.42	4.42	0.0589
Spacing [nm]	17.3	17.3	0.000234
Offset [μm]	0.00	−4.42	–
Min [nm]	–	–	−21
Max [nm]	–	–	37.9
Size	256 Points	256 Lines	251473 Decimals

Table 12. Parameters of the fifth sample generated from the ID card after shapes removal.

Parameter	Axis		
	X	Y	Z
Length [μm]	4.42	4.42	0.0277
Spacing [nm]	17.3	17.3	0.0000358
Offset [μm]	0.00	−4.42	–
Min [nm]	–	–	−9.99
Max [nm]	–	–	17.7
Size	256 Points	256 Lines	775241 Decimals

Table 13. Parameters of the sixth sample generated from the ID card after shapes removal.

Parameter	Axis		
	X	Y	Z
Length [μm]	4.42	4.42	0.0238
Spacing [nm]	17.3	17.3	0.000127
Offset [μm]	0.00	−4.42	–
Min [nm]	–	–	−11.0
Max [nm]	–	–	12.8
Size	256 Points	256 Lines	187494 Decimals

Table 14. Stereometric parameters of the first sample surface with a description for ISO 25178.

ISO 25178		
Height parameters		
Sq [nm]	3.07	Least-squares height of the surface
Ssk	0.447	Asymmetry of the surface
Sku	4.06	Kurtosis of the surface
Sp [nm]	17.0	The maximum height of surface file
Sv [nm]	12.2	The maximum height of the surface cavity
Sz [nm]	29.2	The maximum height of the surface
Sa [nm]	2.4	The arithmetic mean of the surface height
Function parameters		
Smr [%]	100	Field ratio of the surface material
Smc [nm]	3.86	Inverse field ratio of the surface material
Sxp [nm]	4.95	The maximum height of the peak
Spatial parameters		
Sal [μm]	0.0391	The length of the autocorrelation of surface
Str	0.277	The elongation of the surface structure
Std [$^\circ$]	61.7	Directionality of surface structure
Hybrid parameters		
Sdq	0.145	Least-squares gradient of surface
Sdr [%]	1.05	Expanded relationship of the interfacial field of the surface
Function parameters (Volume)		
Vm [μm^3/μm^2]	0.000196	The volume of the material of surface
Vv [μm^3/μm^2]	0.00406	The volume of empty space surface
Vmp [μm^3/μm^2]	0.000196	The volume of the file of material of surface
Vmc [μm^3/μm^2]	0.00263	The volume of the core of the material of surface
Vvc [μm^3/μm^2]	0.00378	The volume of the core of empty space surface
Vvv [μm^3/μm^2]	0.000283	The volume of empty space of cavity surface
Features parameters		
Spd [1/μm^2]	56.1	The density of surface files
Spc [1/μm]	9.79	Arithmetic mean curvature of file of the surface
$S10z$ [nm]	14.3	The height of the ten points of the surface
$S5p$ [nm]	8.67	The height of the five points of the surface
$S5v$ [nm]	5.58	The height of the five cavities of the surface
Sda [μm^2]	0.0263	The field of average vale
Sha [μm^2]	0.0172	Area of the average beacon

Table 15. Stereometric parameters of the first sample surface with a description for EUR 15178N.

EUR 15178N		
Amplitude parameters		
Sa [nm]	2.40	The average arithmetic deviation
Sq [nm]	3.07	The average least-squares deviation
Sz [nm]	27.5	The height of the ten points of the surface
Ssk	0.447	Asymmetry of the surface
Sku	4.06	Kurtosis of the surface
Sp [nm]	17.0	Maximum height of the peak
Sv [nm]	12.2	The maximum depth of the vale
St [nm]	29.2	Total height
Field and volume parameters		
Smr [%]	100	Field ratio of the surface material
Sdc [nm]	6.41	Difference in altitude of the area
Spatial parameters		
Sal [μm]	0.0391	Length of the fastest dissolution of autocorrelation
Str	0.277	The elongation of the surface structure
Std [°]	28.3	Direction of surface structure
Hybrid parameters		
Sdq	0.145	The least-squares gradient
Sdr [%]	1.05	Developed interfacial field
Sds [$1/\mu m^2$]	154	The density of vertices
Ssc [$1/\mu$m]	9.22	Arithmetic mean curvature of the peak
Sfd	2.80	Fractal dimension of the surface
Function parameters		
Sk [nm]	–	Depth of roughness of the core
Spk [nm]	–	The reduced height of the peak
Svk [nm]	–	Reduced depth of the Vale
*Sr*1 [%]	0.00	The upper carrying surface
*Sr*2 [%]	0.00	The lower carrying surface
Spq	–	Least-squares inequation of the plateau
Svq	–	Least-squares inequation of the vale
Smq	–	The material ratio at the transition plateau-valley

Table 16. Table comparing the spatial parameters in agreement with ISO 25178 standard and EUR 15178N.

	Spatial parameters		
Standard	*Str*	*Std*	*Sal*
ISO 25178	0.277	61.7	0.0391
EUR 15178N	0.277	28.3	0.0391

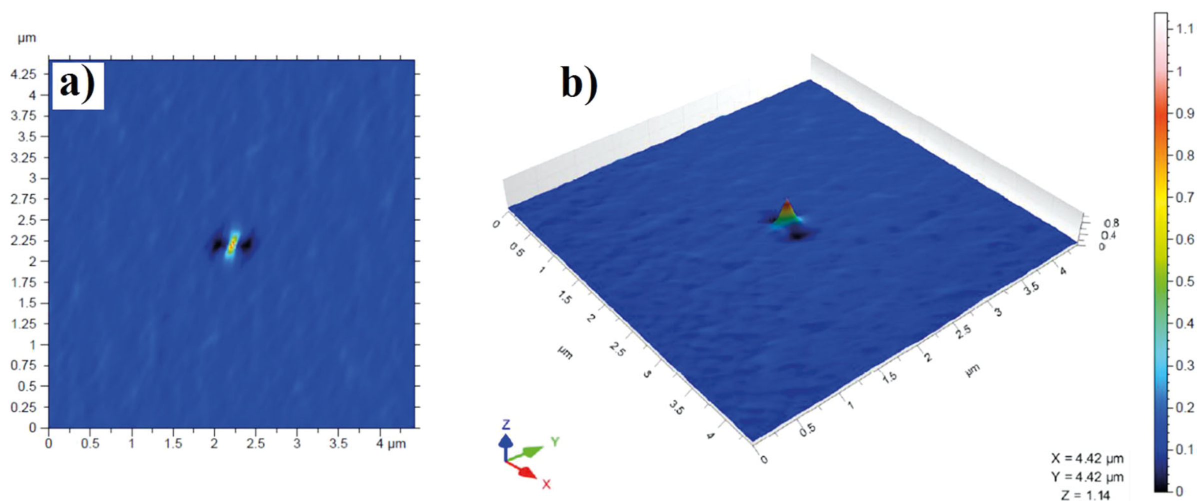

Fig. 4. Peak of autocorrelation using a threshold of 0.2 for the first sample represented in (a) 2D and (b) 3D.

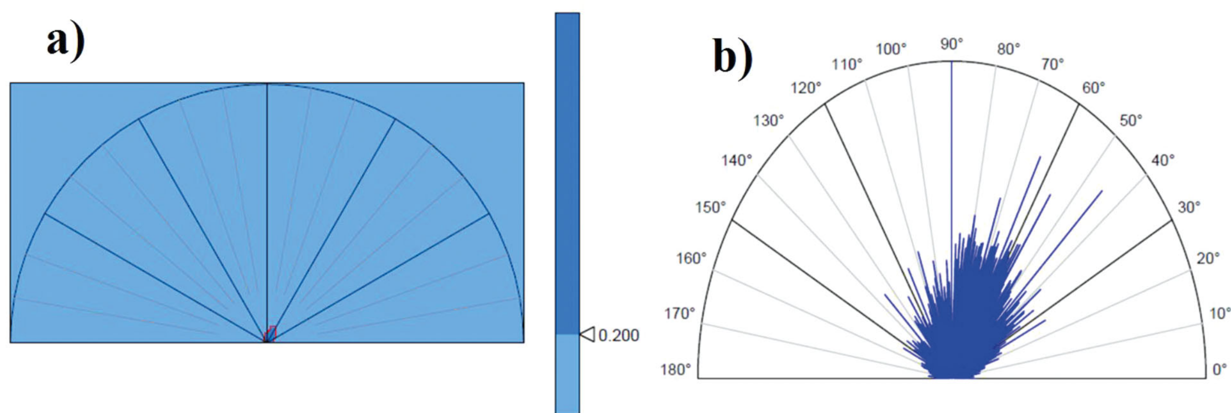

Fig. 5. Diagrams showing the directionality properties of the structure for the first sample with the default threshold of 0.2.

Table 17. Comparison between the directionality properties of the six samples.

Sample	S1	S2	S3	S4	S5	S6
Isotropy (%)	27.7	26.9	42.0	61.6	62.0	53.0
First direction (°)	90.0	63.6	45.0	90.0	135.0	90.0
Second direction (°)	45.0	45.0	56.2	0.15	90.0	135.0
Third direction (°)	63.5	90.0	0.14	45.0	116.0	45.0

Table 18. Height differences for axis Z from each samples.

Parameter	Sample I	Sample II	Sample III	Sample IV	Sample V	Sample VI
Difference in altitude before leveling [nm]	29.0	25.01	38.0	57.5	27.73	23.89
Difference in altitude after leveling [nm]	29.2	24.93	37.5	58.9	27.69	23.80

Table 19. The spatial parameter values according to ISO 25178 for individual measurement data obtained as a result of the study.

	Sample I	Sample II	Sample III	Sample IV	Sample V	Sample VI
Sal [μm]	0.0391	0.0324	0.0508	0.0953	0.0318	0.0314
Str	0.277	0.269	0.420	0.616	0.620	0.530
Std [°]	61.7	73.0	54.5	56.3	120	73.2

Table 20. The spatial parameter values according to EUR 15178N for individual measurement data obtained as a result of the study.

	Sample I	Sample II	Sample III	Sample IV	Sample V	Sample VI
Sal [μm]	0.0391	0.0324	0.0508	0.0953	0.0318	0.0314
Str	0.277	0.269	0.420	0.616	0.620	0.530
Std [°]	28.3	17.0	35.5	33.7	−29.7	16.8

Financial disclosure

Neither author has a financial or proprietary interest in any material or method mentioned.

Competing interests

The authors declare that they have no competing interests.

References

1. C.-H. Ma, J.-H. Huang, H. Chen, Surf. Coat. Technol. **200**, 3868 (2006).
2. W.-J. Chou, G.-P. Yu, J.-H. Huang, Surf. Coat. Technol. **140**, 206 (2001).
3. W.-J. Chou, G.-P. Yu, J.-H. Huang, Surf. Coat. Technol. **149**, 7 (2002).
4. M. Azadi, A.S. Rouhaghdam, S. Ahangarani, H.H. Mofidi, M. Valiei, Adv. Mater. Res. **829**, 476 (2014).
5. Helen E. Rebenne, Deepak G. Bhat, Surf. Coat. Technol. **63**, 1 (1994).
6. Shanyong Zhang, Weiguang Zhu, J. Mater. Process. Technol. **39**, 165 (1993).
7. H. Mofidi, A.S.R. Aghdam, S. Ahangarani, M. Bozorg, M. Azadi, M. Valiei, Mater. Sci. Appl. **5**, 140 (2014).
8. H.H. Mofidi, A.S. Rouhaghdam, S. Ahangarani, M. Bozorg, M. Azadi, Adv. Mater. Res. **829**, 466 (2014).
9. L.E. Toth, *Transition Metal Carbides and Nitrides* (Academic Press, New York, 1971).
10. Ruud P. van Hove, Inger N. Sierevelt, Barend J. van Royen, Peter A. Nolte, BioMed. Res. Int. **2015**, 485975 (2015).
11. Z. Cheng, H. Peng, G. Xie, Y. Shi, Surf. Coat. Technol. **138**, 237 (2001).
12. N. Ghobadi, M. Ganji, C. Luna, A. Ahmadpourian, A. Arman, Opt. Quantum Electron. **48**, 467 (2016).
13. K. Xu, J. Chen, R. Gao, J. He, Surf. Coat. Technol. **58**, 37 (1993).
14. D. Dastan, S.L. Panahi, A.P. Yengantiwar, A.G. Banpurkar, Adv. Sci. Lett. **22**, 950 (2016).
15. Y. Wang, A. Capretti, L. Dal Negro, Opt. Mater. Express **5**, 2415 (2015).
16. Guo-ran Li, Feng Wang, Qi-wei Jiang, Xue-ping Gao, Pan-wen Shen, Angew. Chem. Int. Ed. **49**, 3653 (2010).
17. A. Achour, M. Chaker, H. Achour, A. Arman, M. Islam, M. Mardani, M. Boujtita, L. Le Brizoual, M.A. Djouadi, T. Brousse, J. Power Sources **359**, 349 (2017).
18. Amine Achour, Raul Lucio Porto, Mohamed-Akram Soussou, Mohammad Islam, Mohammed Boujtita, Kaltouma Ait Aissa, Laurent Le Brizoual, Abdou Djouadi, Thierry Brousse, J. Power Sources **300**, 525 (2015).
19. A. Achour, R. Lucio-Porto, M. Chaker, A. Arman, A. Ahmadpourian, M.A. Soussou, M. Boujtita, L. Le Brizoual, M.A. Djouadi, T. Brousse, Electrochem. Commun. **77**, 40 (2017).
20. B. Bogdanović, M. Felderhoff, S. Kaskel, A. Pommerin, K. Schlichte, F. Schüth, Adv. Mater. **15**, 1012 (2003).
21. Stefan Kaskel, Klaus Schlichte, Tobias Kratzke, J. Mol. Catalysis A **208**, 291 (2004).
22. M. Birkholz, K.-E. Ehwald, D. Wolansky, I. Costina, C. Baristiran-Kaynak, M. Fröhlich, H. Beyer, A. Kapp, F. Lisdat, Surf. Coat. Technol. **204**, 2055 (2010).
23. S. Ramazanov, Ş. Ţălu, D. Sobola, S. Stach, G. Ramazanov, Superlattices Microstruct. **86**, 395 (2015).
24. Ş. Ţălu, S. Stach, S. Valedbagi, S. Mohammad Elahi, R. Bavadi, Mater. Sci. Poland **33**, 137 (2015).
25. T. Larsson, H.O. Blom, C. Nender, S. Berg, J. Vacuum Sci. Technol. A **6**, 1832 (1988).

26. A. Arman, Ş. Ţălu, C. Luna, A. Ahmadpourian, M. Naseri, M. Molamohammadi, J. Mater. Sci. **26**, 9630 (2015).
27. S. Stach, D. Dallaeva, Ş. Ţălu, P. Kaspar, P. Tománek, S. Giovanzana, L. Grmela, Mater. Sci. Poland **33**, 175 (2015).
28. Siegfried Hofmann, Thin Solid Films **191**, 335 (1990).
29. N. Ouldhamadouche, A. Achour, K. Ait Aissa, M. Islam, A. Ahmadpourian, A. Arman, M.A. Soussou, M. Chaker, L. Le Brizoual, M.A. Djouadi, Thin Solid Films **622**, 23 (2017).
30. Ş. Ţălu, S. Stach, A. Méndez, G. Trejo, M. Ţălu, J. Electrochem. Soc. **161**, D44 (2014).
31. Ş. Ţălu, *Micro and nanoscale characterization of three dimensional surfaces. Basics and applications* (Napoca Star Publishing House, Cluj-Napoca, Romania, 2015).
32. S. Stach, Ż. Garczyk, Ş. Ţălu, S. Solaymani, A. Ghaderi, R. Moradian, N.B. Nezafat, S.M. Elahi, H. Gholamali, J. Phys. Chem. C **119**, 17887 (2015).
33. Ş. Ţălu, A.J. Ghazai, S. Stach, A. Hassan, Z. Hassan, M. Ţălu, J. Mater. Sci. **25**, 466 (2014).
34. Ş. Ţălu, R.P. Yadav, A.K. Mittal *et al.*, Opt. Quantum Electron. **49**, 256 (2017).
35. Ş. Ţălu, S. Stach, D. Raoufi, F. Hosseinpanahi, Electr. Mater. Lett. **11**, 749 (2015).
36. N. Ghobadi, M. Ganji, C. Luna, A. Arman, A. Ahmadpourian, J. Mater. Sci. **27**, 2800 (2016).
37. S. Stach, W. Sapota, Ş. Ţălu, A. Ahmadpourian, C. Luna, N. Ghobadi, A. Arman, M. Ganji, J. Mater. Sci. **28**, 2113 (2017).
38. MountainsMap 7 Software (Digital Surf, Besançon, France) available at: `http://www.digitalsurf.fr` (last accessed March 10th, 2017).
39. ISO 25178-2, *2012 Geometrical product specifications (GPS) – Surface texture: Areal – Part 2: Terms, definitions and surface texture parameters* (2012) `http://www.iso.org` (last accessed March 10th, 2017).